www.elsevier.com/locate/yjtbi

Multi-scale homogenization of blood flow in 3-dimensional Human cerebral microvascular networks

Wahbi K. El-Bouri, Stephen J. Payne

PII: S0022-5193(15)00239-8
DOI: http://dx.doi.org/10.1016/j.jtbi.2015.05.011
Reference: YJTBI8193

To appear in: *Journal of Theoretical Biology*

Received date: 20 January 2015
Revised date: 10 April 2015
Accepted date: 6 May 2015

Cite this article as: Wahbi K. El-Bouri, Stephen J. Payne, Multi-scale homogenization of blood flow in 3-dimensional Human cerebral microvascular networks, *Journal of Theoretical Biology,* http://dx.doi.org/10.1016/j.jtbi.2015.05.011

Title Page

Multi-scale homogenization of blood flow in 3-dimensional human cerebral microvascular networks

Authors: Wahbi K. El-Bouri and Stephen J. Payne

Address: Department of Engineering Science, Institute of Biomedical Engineering, University of Oxford, Parks Road, Oxford OX1 3PJ, UK

Abbreviated Title: Homogenization of blood flow in microvascular networks

Correspondence: Wahbi K. El-Bouri, Department of Engineering Science, Institute of Biomedical Engineering, University of Oxford, Parks Road, Oxford OX1 3PJ, UK

Tel No. +44 (0)1865 617696

Fax No. +44 (0)1865 617703

E-mail: wahbi.el-bouri@eng.ox.ac.uk (corresponding author); stephen.payne@eng.ox.ac.uk

Abstract and Key Terms

The microvasculature plays a crucial role in the perfusion of blood through cerebral tissue. Current models of the cerebral microvasculature are discrete, and hence only able to model the perfusion over small voxel sizes before becoming computationally prohibitive. Larger models are required to provide comparisons and validation against imaging data. In this work, multi-scale homogenization methods were employed to develop continuum models of blood flow in a capillary network model of the human cortex. Homogenization of the local scale blood flow equations produced an averaged form of Darcy's law, with the permeability tensor encapsulating the capillary bed topology. A statistically accurate network model of the human cortex microvasculature was adapted to impose periodicity, and the elements of the permeability tensor calculated over a range of voxel sizes. The permeability tensor was found to converge to an effective permeability as voxel size increased. This converged permeability tensor was isotropic, reflecting the mesh-like structure of the cerebral microvasculature, with off-diagonal terms normally distributed about zero. A representative elementary volume of 375 μm, with a standard deviation of 4.5 % from the effective permeability, was determined. Using the converged permeability values, the cerebral blood flow was calculated to be around 55 mL min^{-1} $100g^{-1}$, which is in very close agreement with experimental values. These results open up the possibility of future multi-scale modelling of the cerebral vascular network.

Key Terms: capillary network; continuum model; cerebral blood flow; microvessels; perfusion

1. Introduction

A constant supply of blood is essential to keeping the brain in a healthy functioning state. The brain takes up around 2 % of the mass of an average human body, yet consumes 20 % of the oxygen supply of the whole body (Clarke and Sokoloff, 1999). This makes it particularly vulnerable to severe reductions in blood supply, with damage occurring within tens of seconds. Any mismatch between the metabolic rate in the brain cells and oxygen supply leads to localised damage of tissue, known as ischemia, and eventual infarction if the supply of blood, and hence oxygen, is not restored. On a large scale, this is often referred to as a stroke.

Increasingly, the underlying microvascular architecture is recognised as being key to the perfusion rate and the delivery of oxygen to surrounding tissue (Cassot et al., 2006; Lauwers et al., 2008; Reichold et al., 2009). Hemodynamically based functional imaging techniques, such as fMRI, make use of the coupling between neuronal activity and local increases in blood flow and metabolism. However, the spatial resolution of such imaging techniques is not high enough to pick out the microvasculature and its effects on perfusion. As a result, little information is available on the interplay between the microvascular topology and tissue-scale perfusion. Characterising this interplay, and the response of the vascular system to hemodynamic disturbances, is likely to help to improve the treatment of vascular diseases.

In order to aid with understanding blood flow in the brain, a number of models have been built of blood and oxygen transport through the main groups of vessels in the vasculature. These models are most often discrete networks with 1-dimensional blood flow

through the vessels. On the local scale, these models are useful for analysing perfusion and oxygen transport through individual vessels and the surrounding extracellular space. Secomb et al. (Secomb et al., 2000) and Fang et al. (Fang et al., 2008) have developed models of blood and oxygen transport that can be applied to any 3-dimensional network, and which were applied to transport in the rat cortex. Similarly, others have reconstructed a rat cortex network from experimental data, using it to investigate the effects of local vascular dilation and occlusion (Reichold et al., 2009). Lorthois et al. applied the transport models to a reconstructed network from the human cerebral cortex (Lorthois et al., 2011). The network was reconstructed from experimental data (Cassot et al., 2006). Su et al. also used these cerebral cortex data, but rather than reconstruct the observed network, they developed a statistical algorithm to fit morphometric parameters and statistically to model the microvasculature (Su et al., 2012). Such an algorithm is valuable as it bypasses the labour intensive and time-consuming method of experimentally extracting the structure of the microvasculature at each section in the brain. Additionally, such statistical algorithms are easily adaptable for varying statistical parameters at different cerebral locations.

However, all of these models are currently only computationally reasonable for small tissue sections. Building larger models so that accurate comparisons can be made with imaging data becomes very difficult using current discrete modelling techniques. Boundary conditions of imaged sections are also unknown and have been shown to have a strong effect on flow properties (Lorthois et al., 2011). This makes it very difficult to determine the effect of the microvasculature on tissue-scale fluid transport. In order to gain a more comprehensive understanding of the perfusion and pathophysiological conditions

associated with the vasculature, a mathematically rigorous multi-scale model will be required, which is not currently achievable.

Continuum-based mathematical modelling techniques, specifically homogenization, aim to deal with these issues. Homogenization is an averaging technique which derives macro-scale models using micro-scale models, assuming that there is scale separation between the two sizes and that the micro-scale model is periodic. Using such methods results in the discrete micro-scale representation being replaced with averaged integral quantities of the capillary bed valid over the larger region of interest, reducing the computational cost substantially. A key advantage of this continuum approach is that the results are independent of the choice of boundary condition.

Shipley and Chapman used these mathematical averaging techniques on a leaky capillary bed to derive an averaged macroscopic Darcy flow model (Shipley and Chapman, 2010). The permeability tensor of this flow model is what links the capillary-scale topology to macro-scale blood flow, and is the property of interest when scaling up discrete models. Characterizing this tensor allows us to build larger continuum models of the cerebral microvasculature. The idea of scale separation introduces the concept of a representative elementary volume (REV). This is generally defined as the minimum volume within which the property of interest remains relatively constant (Bear, 1988). Therefore, determining the REV of a network is important to minimise computation time. Smith et al. have previously used the averaging techniques derived by Shipley and Chapman on a model of non-leaky rat myocardial capillaries (Smith et al., 2014).

In this paper, we adapt the discrete model developed by Su et al. in order to generate periodic, statistically accurate, 3-dimensional models of the cerebral microvasculature for

the first time. The techniques developed by Shipley and Chapman for capillary networks in tumours are used to derive macro-scale flow equations for non-leaky capillaries, with no slip boundary conditions on the capillary walls. These are used to calculate the permeability tensors of various voxel sizes in order to determine convergence of the permeability. From the converged permeability a REV can be calculated for a given error tolerance.

2. Materials and Methods

2.1 Homogenization of the Capillary Network

The same homogenization methods are used here, as in Shipley and Chapman, to derive the continuum equations for a normal cerebral vasculature. The model of the brain tissue proposed here has two distinct phases: the capillaries and the interstitium. The interstitium, comprised of cells and extracellular space, is assumed to be a porous medium due to the large size of the capillaries in comparison to the inter-cell separation. Blood flow in the capillaries is assumed to be incompressible, of constant hematocrit, and to obey Stokes flow (viscous dominated at the capillary-scale). The validity of assuming constant hematocrit will be examined in the '*Discussion*'. It is also assumed that there is negligible leakage of blood between the capillaries and interstitium, and no-slip, no-leak boundary conditions are imposed for the blood velocity at capillary walls. As a result, the system of equations to homogenize on the micro (capillary) scale is:

$$-\nabla p_c + \mu \nabla^2 \mathbf{u}_c = 0 \quad \text{in } \Omega_c \tag{1}$$

$$\nabla . \mathbf{u}_c = 0 \quad \text{in } \Omega_c \tag{2}$$

$$\mathbf{u}_c.\boldsymbol{\tau} = 0 \quad \text{on } \Gamma_c \tag{3}$$

$$\mathbf{u}_c.\mathbf{n} = 0 \quad \text{on } \Gamma_c \tag{4}$$

where subscript c refers to the capillary domain, Ω_c is the capillary volume, Γ_c is the capillary wall surface, ρ is the density of blood, $\mathbf{u}_c$ is the blood velocity, μ is the blood viscosity, p_c is the blood pressure, and $\boldsymbol{\tau}$ and $\mathbf{n}$ are the tangential and normal unit vectors respectively.

A small parameter ε, defined as the ratio of the micro and macro length scales, is introduced by non-dimensionalizing the set of equations using the following characteristic values:

$$\mathbf{u}_c = U\mathbf{u}_c', \;\; p_c = \frac{\mu LU}{d^2}p_c' + p_0, \;\; \mathbf{X} = d\mathbf{X}' \tag{5}$$

where U, L, and d are characteristic values of velocity, macro length scale, and micro length scale respectively, $\mathbf{X}$ is the micro length variable, p_0 is a pressure offset, and the prime variables are non-dimensional forms of the original variables. Substituting the non-dimensional variables from (5) into (1), multiplying by $d^3/\mu LU$, and dropping the primes gives:

$$-\nabla p_c + \varepsilon\nabla^2\mathbf{u}_c = 0 \quad \text{in } \Omega_c \tag{6}$$

where ε is defined as:

$$\varepsilon = \frac{d}{L} \tag{7}$$

Assuming well-separated micro and macro length scales and a periodic microstructure, an asymptotic expansion is performed for the blood pressure and velocity in terms of the

small parameter ε – as previously detailed (Shipley and Chapman, 2010). The assumption of periodicity is necessary, particularly in multi-dimensional systems, due to the need to remove secular terms. Periodicity is a mathematical tool regularly used in homogenization to simplify the removal of secular terms (Auriault et al., 2009; Holmes, 2013; Shipley and Chapman, 2010). The validity of this assumption for cerebral microvascular networks is discussed later. The end result of the homogenization is an equation dependent only on the macro-scale with averaged coefficients. It is these coefficients which are determined from solving the local scale problem.

Performing the homogenization technique (see Appendix A) under the given assumptions leads to the volume averaged form of Darcy's law on the macro-scale:

$$\langle \mathbf{u}_c^{(0)} \rangle_{\Omega_c} = -\mathbf{K} \nabla p_c^{(0)} \tag{8}$$

where $\nabla p_c^{(0)}$ is the leading order macro-scale pressure gradient, $\mathbf{K}$ is the permeability tensor, and $\langle \mathbf{u}_c^{(0)} \rangle_{\Omega_c}$ is the volume averaged leading order velocity over the capillary domain. It has been shown that, to leading order, the volume averaged velocity is equivalent to a surface mean velocity (Darcy Flux) (Auriault et al., 2009; Durlofsky, 1991). Therefore (8) can be rewritten as:

$$\langle \mathbf{u}_c^{(0)} \rangle_{\Gamma} = -\mathbf{K} \nabla p_c^{(0)} \tag{9}$$

where $\langle \mathbf{u}_c^{(0)} \rangle_{\Gamma}$ is the surface mean flux taken at the outflow boundaries of the periodic voxel over which we are averaging.

The homogenized permeability tensor $\mathbf{K}$ is important as this encapsulates the geometry of the periodic substructure. It is an averaged coefficient tensor, calculated by

solving the micro cell problem. Determining the converged values of the elements of the tensor allows us to build 'scaled-up' models of blood flow in the cerebral microvasculature.

2.2 Calculation of the Permeability Tensor

In order to determine the averaged permeability tensor, a periodic boundary value problem must be solved over the periodic micro cell of the capillary network. Assuming the radial and swirl components of the blood velocity at the capillary-scale to be zero, and fully developed flow, then the blood follows Poiseuille flow. Integrating the velocity profile of each capillary over the cross-section of capillary m leads to Poiseuille's equation:

$$\boldsymbol{q}_m^j = \frac{\pi r_m^4}{8\mu_m}\left(\frac{\Delta P_m^j}{L_m}\right), \ j = 1,2,3 \tag{10}$$

where $\boldsymbol{q}_m^j$ is the flux through capillary m, r_m and L_m are the radius and length of the capillary respectively, and ΔP_m^j is the local pressure drop along the capillary length. The viscosity law of Pries et al. is used to account for non-Newtonian rheology for a constant discharge hematocrit of 0.45 (Pries et al., 1994).

Since the left hand side of (9) is a surface mean, it can be calculated by summing the capillary flow rates cutting through a surface of the voxel and dividing by the area of that surface. Therefore the elements of the permeability tensor can be calculated as such:

$$K_{ij} = \frac{\Sigma \boldsymbol{q}_{m,surf}^j}{\Gamma^j \nabla p^i}, \ \ i,j = 1,2,3 \tag{11}$$

where $\boldsymbol{q}_{m,surf}^j$ is a surface outflow node in the jth direction and Γ^j is the cube outflow surface area. As a result three independent pressure gradients are required in order to

determine $\mathbf{K}$ for the 3-dimensional structure of the cerebral microvasculature. In our case i, j refer to Cartesian co-ordinates. As an example, if we wish to calculate K_{11} then a pressure gradient is imposed in the x-direction, the total flow rate through the Γ_1 surface is calculated, and divided by the surface area Γ_1 and the pressure gradient in the x-direction. In order to calculate the cross flows in the y and z directions, the same procedure is followed but over the Γ_2 and Γ_3 surfaces respectively, yielding K_{12} and K_{13}. Imposing pressure gradients in the y and z directions produces the second and third rows of the tensor respectively, and hence the full 3x3 permeability tensor.

2.3 Application to Synthetic Cerebral Microvascular Networks

The network generation algorithm developed by Su et al. is used here in order to generate statistically accurate models of the cerebral microvasculature. The homogenization theory already detailed is then applied to this model to calculate the permeability tensor. The model is based on the morphometric data obtained by Cassot et al. In Cassot's study, quantitative morphometric information was extracted from the collateral sulcus in the right temporal lobe using Indian ink and confocal laser microscopy to analyse sample sections. The vessel density, length distribution of vessels, distribution of the radii of the vessels, and average connectivity were some of the parameters found which provide enough information to generate statistically accurate models of the cerebral vasculature.

The algorithm, proposed by Su et al., uses a modified spanning tree method (MSTM), where two spanning trees are generated from randomly seeded nodes on a given voxel which then merge to form a random capillary network. The diameters of the capillaries are assumed to be normally distributed with a mean of 6.23 μm and a standard deviation of 1.3 μm, in accordance with experimental data (Cassot et al., 2006). In order to fit the length

distribution of the vessels found in Cassot et al., filters are then applied, which remove and add vessels depending on their length.

The assumption of periodicity made during the homogenization process means it is necessary to modify this model. It is currently not spatially periodic, nor does it have periodicity of blood flow through opposing surfaces of the voxel. Therefore, the model is modified here to introduce spatial and flow periodicity.

In order to impose spatial periodicity, the surfaces of the voxel must be symmetric. This is achieved by randomly seeding three non-opposite faces with nodes and copying their co-ordinates over to their opposing faces. The internal nodes of the voxel are seeded randomly. Each surface node has one capillary connected to it from the internal network. Capillaries attached to opposing surface nodes are summed to form one long capillary. Along with the filters used by Su et al., this allows for the generated models to statistically fit the experimental data despite the constraint of spatial periodicity. A typical spatially periodic voxel is shown in Fig. 1.

Various voxel sizes are generated in order to determine how the permeability of the cerebral network varies with size. In order to 'scale-up' to larger voxel sizes a base voxel must be chosen. As there can only be an integer number of nodes, the size of the periodic base voxel is limited by being able to accurately fit the experimental data whilst having one surface node on each face. It was found that a 125 µm cube with one surface node on each face is able to match the length distribution of the capillary network, as well as the segment density (in the range 7219 – 8817 /mm^3 (Cassot et al., 2006)). Therefore, one surface node on a 125 µm cube is deemed to be an acceptable base voxel. Larger cubes can be built by stacking 125 µm cubes together.

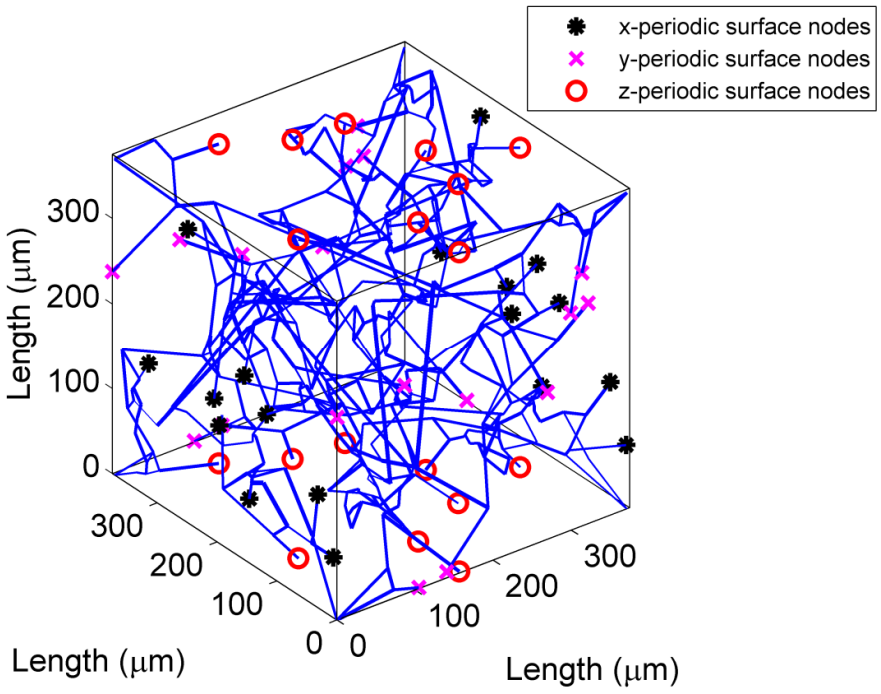

FIG 1. Typical cerebral capillary network, generated in a 375 μm cube with the additional constraint of spatial periodicity.

Finally, the flow over opposing faces of the voxel must also be periodic, i.e. the total influx over one face must be equal and opposite to the outflux over the opposing face. This is achieved by using wrap-around boundary conditions on the four faces over which the pressure gradient is not applied.

The capillary networks are simulated 500 times for every cube size so that the average length distribution of the capillaries matches that observed by Cassot et al. The 10 cube sizes used ranged in length from 125 - 625 μm (see Table 1). Cube sizes not multiples of 125 μm had the number of surface nodes rounded down to the nearest whole integer. The sizes chosen were such that the rounding error of the surface nodes was kept to a minimum, whilst also giving a good spread of values in the range of sizes being simulated.

Cube sizes larger than 625 µm were found to be extremely computationally expensive to simulate, therefore 625 µm was chosen as the upper bound of the sizes.

Cube Size (µm)	Mean Segment Density (/mm^3)	Mean Segment Length (µm)	No. Surface Nodes (/face)
125	8621 ± 939	57.5 ± 5.8	1
180	7744 ± 697	57.2 ± 3.2	2
250	7991 ± 479	57.2 ± 1.9	4
300	7685 ± 327	53.5 ± 1.3	5
375	7763 ± 229	56.4 ± 0.9	9
425	8048 ± 209	54.2 ± 0.7	11
450	8162 ± 184	54.6 ± 0.6	12
500	7934 ± 164	56.1 ± 0.6	16
550	8272 ± 143	54.9 ± 0.5	19
625	8115 ± 119	55.0 ± 0.4	25

TABLE 1: Table of the mean segment densities, mean segment length, and surface nodes of the 10 periodic cube sizes used to model the cerebral capillary network.

2.4 Calculation of the Representative Elementary Volume

The idea of scale separation introduces the concept of a representative elementary volume (REV). Within the range of the REV the macroscopic permeability coefficient does not change significantly. The REV contains a large enough number of capillary-scale heterogeneities that the permeability coefficient calculated from it can be considered to be the effective permeability coefficient on the macro-scale (Renard and de Marsily, 1997).

As the periodic voxel simulation size increases, $\varepsilon \rightarrow 0$, and hence the permeability coefficient tensor asymptotically tends to the effective macro-scale permeability. It is therefore expected that as voxel size increases, the calculated permeability will tend to a

converged asymptotic macro permeability, similar to that observed by Smith et al. for their simulations of capillary networks in the rat myocardium (Smith et al., 2014).

In order to determine the converged permeability of each element in the tensor, the root mean square error between the variation of permeability with cube size and a curve of best fit of the form:

$$K_{mean} = \Delta K e^{-\frac{L}{L_{ch}}} + K_{eff} \quad (12)$$

was minimised, where K_{mean} is the mean permeability at every cube size, L the cube length, L_{ch} a characteristic length, ΔK a stretch coefficient, and K_{eff} the effective, or macro, permeability. The average permeability values at each cube size for each element in the tensor is plotted, and the line of best fit provides a functional equation of how the permeability varies with cube size. This form of equation was chosen to fit the data as it was a simple fit with few parameters. ΔK, L_{ch}, and K_{eff} were found using the *fminsearch* function on MATLAB.

It is then possible to calculate the REV for an acceptable error margin by comparing the calculated permeability of a given cube size with the converged permeability, K_{eff}. Determining the minimum REV is important in order to minimise computation time when scaling up models.

3. Results

3.1 Periodic Network Generation

The cube sizes used, along with the average segment density, are listed in Table 1. As can be seen, all the mean segment values lie within the range 7219 - 8817 /mm^3 found experimentally (Cassot et al., 2006). The distribution of the number of segments for each cube are normally distributed over the samples (all p-values > 0.05), except for the 125 µm cube. Therefore the segment density at each cube size can be characterised by a mean and standard deviation. The average length distribution of the simulated capillary networks provides a good match to the experimental results of Cassot et al., despite the additional constraint of periodicity (see Fig. 2). The mean capillary length density – the product of the mean segment density and the mean length – ranged from 411 – 496 /mm^2.

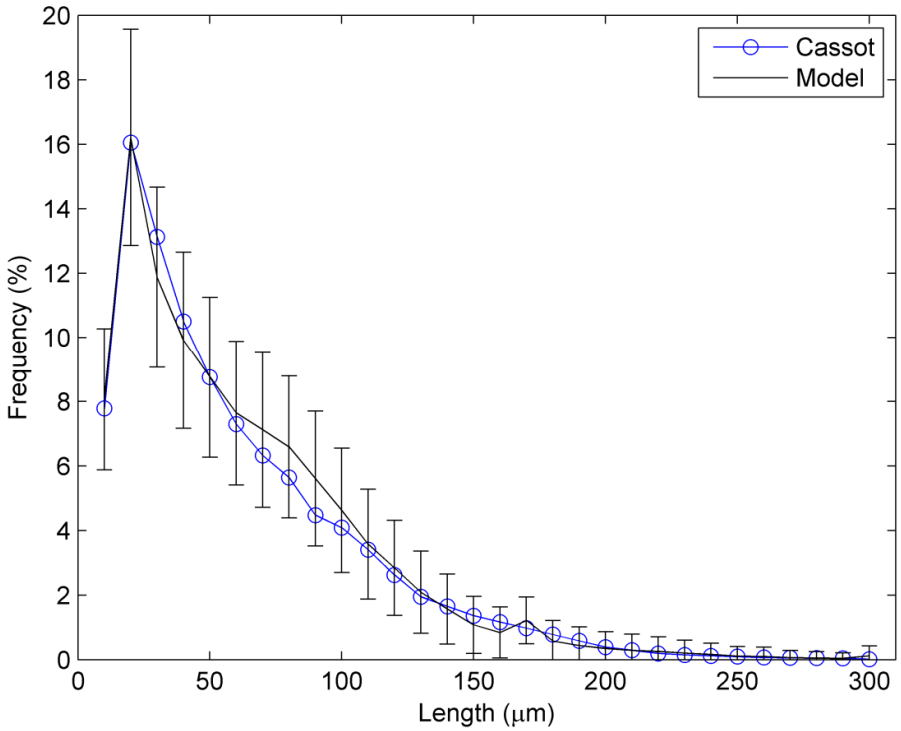

FIG 2: Vessel length distribution of a periodic 250 µm voxel compared with experimental data converted from Cassot et al. (Cassot et al., 2006)

3.2 Permeability of Capillary Networks

All elements of the permeability tensor were normally distributed at each cube size bar those for the 125 µm cube. This was due to the very small number of segments in this voxel size (average of 16) which effectively meant there was a discrete distribution of permeability values. As a result, the results of the 125 µm cube are omitted from the rest of the work. The diagonal terms of the permeability tensor all displayed a decreasing permeability as the cube size increased. The permeability appeared to converge for all three diagonal terms (Fig. 3). The exponential line of best fit (12) was applied over cube sizes ≥ 180 µm. The converged permeability values, K_{eff} were found for K_{11}, K_{22}, and K_{33} to be 4.26 x 10^{-4} mm^3 s kg^{-1}, 4.31 x 10^{-4} mm^3 s kg^{-1}, and 4.27 x 10^{-4} mm^3 s kg^{-1} respectively (the values of ΔK, L_{ch}, and K_{eff} are given in Table 2). The difference in the three diagonal values was < 1.2 % indicating isotropy of the tensor. This mirrors the underlying "mesh or net-like structure" (Cassot et al., 2006) of the cerebral microvasculature, which appears random and isotropic.

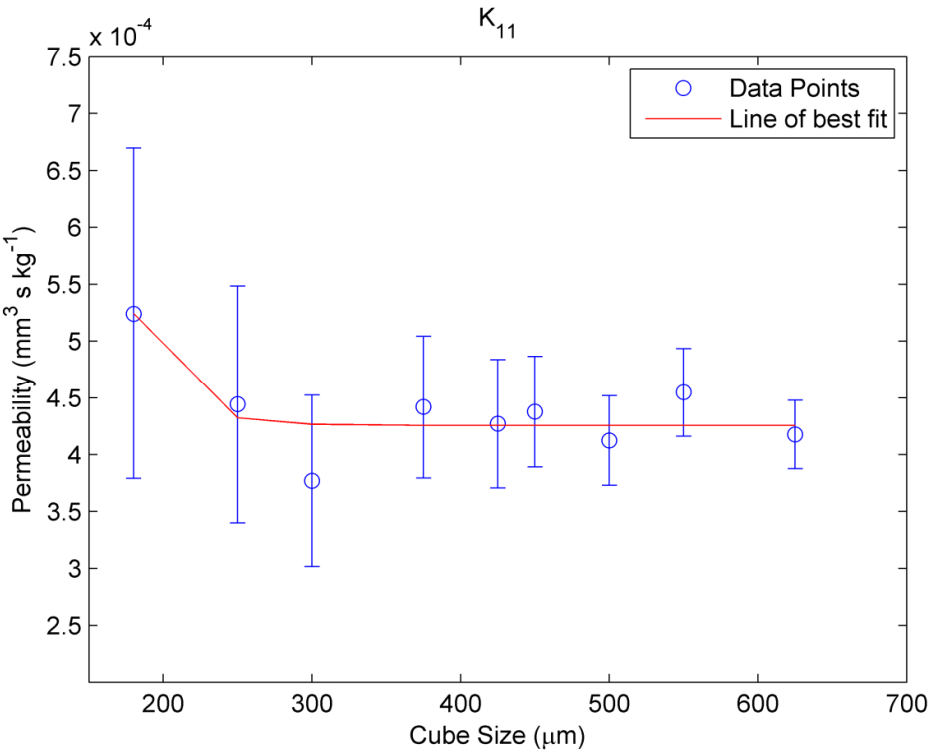

FIG 3: Error-bar plot of the K_{11}term of the permeability tensor. Lines of best fit pass through the error-bars of all cube sizes. The plots of K_{22} and K_{33} are similar.

Simulations over 180 µm, 375 µm, and 625 µm voxel sizes gave mean K_{33} values of (5.35 ± 1.58) x 10^{-4} mm^3 s kg^{-1}, (4.50 ± 0.63) x 10^{-4} mm^3 s kg^{-1}, and (4.20 ± 0.31) x 10^{-4} mm^3 s kg^{-1}. The magnitudes of the errors in these values from the converged permeability (K_{eff}) range from around 25 % to 1.6 %. This is in contrast to the error in the mean calculated by Smith et al. which has a maximum value of around 70 % for a 100 x 100 x 21.6 μm^3 voxel (Smith et al., 2014). The lack of a sharp increase in permeability at smaller cube sizes is likely to be due to the more random, isotropic nature of the cerebral microvasculature, as opposed to the more aligned myocardial capillaries modelled by Smith et al. It is also likely that the much larger density of the longitudinally aligned myocardial capillaries will have partially accounted for this difference. The diagonal terms of the permeability matrix were

found to be an order of magnitude smaller than those measured by Smith et al. for capillaries aligned parallel to the epicardial surface.

	K_{eff} (mm^3 s kg^{-1}) x10^{-4}	ΔK (mm^3 s kg^{-1}) x10^{-4}	L_{ch} (μm)
K_{11}	4.26	1.03	25.9
K_{12}	-0.019	3.96	3.96
K_{13}	-0.0067	0.76	19.7
K_{21}	-0.026	4.13	3.76
K_{22}	4.31	0.096	42.8
K_{23}	0.037	-0.0014	134
K_{31}	0.00025	0.71	18.6
K_{32}	0.050	-0.0015	133
K_{33}	4.27	0.158	36.2

TABLE 2: Parameters of the lines of best fit for the nine permeability tensor elements.

The off-diagonal terms were found to be on average two orders of magnitude smaller than the diagonal terms, indicating that the majority of blood flow occurs in the direction of the pressure gradient. The off-diagonal pairs ([K_{12} , K_{21}], [K_{13} , K_{31}], [K_{23} , K_{32}]) had similar lines of fit which all appeared to converge towards a mean of zero. A t-test was performed to determine whether the off-diagonal terms were distributed normally about a mean of zero. All 6 terms returned a p-value > 0.05; hence the hypothesis that the mean was zero could be accepted. Any deviations from zero were purely due to random variations in construction of the networks.

The off-diagonal pairs were not perfectly symmetric, with slightly differing parameters and converged permeabilities for the lines of best fit (Table 2). However, it is

expected that as the number of simulations for each cube size increases, the off-diagonal pairs will become symmetric. Smith et al. found that the off-diagonal pair for the myocardial permeability tensor had a mean permeability of order 10^{-8} mm^3 s kg^{-1}. This is in contrast to the larger off-diagonal mean found in this study, of order 10^{-6} mm^3 s kg^{-1}. This is likely due to the ordered nature of the simulated myocardial capillary network which had orthogonal connections between principal direction and cross-flow capillaries. In the cerebral microvasculature the capillaries can be aligned in any direction in 3-dimensions, thus increasing the amount of cross-flow.

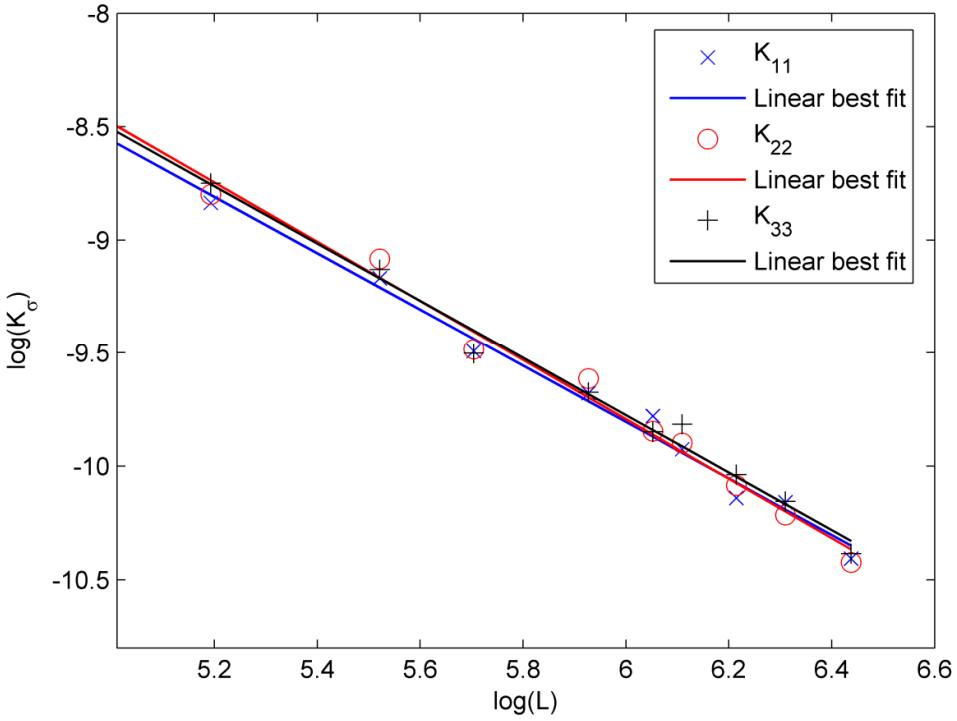

FIG 4: Log-log plot of the standard deviation of the diagonal permeability terms over cube size.

The standard deviation of the diagonal terms dropped linearly with increasing cube size on a log-log plot (Fig. 4). The standard deviation of the off-diagonal terms similarly

displayed a linear drop on a log-log plot. Therefore the standard deviations drop according to a power law as expected. In comparison to the cross-flow standard deviation, the diagonal standard deviations have a steeper drop. The cross-flow standard deviation is almost symmetric, and it is expected that as the number of simulations is increased it will become symmetric.

3.3 Perfusion Estimation

The permeability calculations can be validated, in a similar fashion to Smith et al., using experimental cerebral blood flow (CBF) measurements. Assuming that the pressure gradient is linear across the capillary bed, the perfusion ($\mu m^3\ s^{-1}$) into a region of the brain can be estimated by integrating the Darcy velocity over a cross-sectional area A (μm^2). If the Darcy velocity is parallel to the principal axis over which the pressure gradient is imposed then:

$$Perfusion = K_{ii} \times \frac{\Delta p}{l} \times 0.133 \times 10^{-3} \times A \tag{13}$$

where the factor 0.133×10^{-3} converts from mmHg to kg $\mu m^{-1}\ s^{-2}$, K_{ii} is in kg μm^3 s kg^{-1}, and Δp is a uniform pressure drop of 18 mmHg (Lorthois et al., 2011) over a pre-capillary arteriolar post-capillary venular path length of $l \approx 340$ µm (Sakadžić et al., 2014). Perfusion can also be related to the CBF using the following equation:

$$Perfusion = \frac{\mathrm{CBF}}{60} \times \frac{\rho}{100} \times A \times l \tag{14}$$

where ρ = 0.96 g cm^{-3} and is the cerebral density (Dekaban and Sadowsky, 1978; Lüders et al., 2002), the factor of 60 converts from min to s, and the factor of 100 converts from g to 100g. Substituting Eqn. (14) into (13) using the converged permeability values of K_{11}, K_{22},

and K_{33} yielded a CBF in the range 55.1 – 55.8 mL min^{-1} $100g^{-1}$. These results are within the range, and very close to the mean, of the CBF values observed experimentally of 54.7 ± 6.1 mL min^{-1} $100g^{-1}$ (Obrist et al., 1967).

4. Discussion

In this paper, we homogenized a statistically accurate 3-dimensional model of the human cerebral microvascular network in a portion of the temporal lobe. It was found that the permeability of the capillaries in the three principal directions was highly isotropic, with less than 1.2 % variation in their converged values. This was due to the "mesh-like" structure of the capillary network, and confirms that when modelling the cerebral microvasculature a 2-dimensional simplification of the model is not a valid assumption, unlike when modelling coronary capillary networks (Smith et al., 2014).

The off-diagonal permeability was found to be on average two orders of magnitude smaller than the permeability of the principal terms. This indicates that there was very little crossflow in the capillary network, despite its strongly interconnected nature. The standard deviation of the permeability tensor elements dropped according to a power law. This drop of the standard deviation with cube size is useful in characterising the capillary network.

The converged values of the diagonal permeability terms were found using an exponential line of best fit. The line of best fit passed through every cube size's standard deviation error-bar. The converged values are of use when determining what size REV should be used. The choice is of course application dependent. When choosing, there is a trade-off between computational cost of generating the periodic sub-structure, and the

maximal tolerated deviation, or error, from the converged permeability. The REV should also be of a sensible size relative to any clinical data that are being used to validate the model. If attempting to compare the model with perfusion imaging data, which usually have voxel sizes of the order of mm, then the REV should be smaller than the in-plane resolution of the imaging data. For a 375 µm cube the average error is found to be 4.5 % in this study. This drops to 3.5 % at 500 µm and 1.7 % at 625 µm. Larger cube sizes however require greater computational effort. Therefore on balance it was decided that the 375 µm cube, with an error of 4.5 %, was an acceptable REV for future study. The REV we have calculated is well below typical MRI resolution, and hence can be used with MRI perfusion data for validation.

Reichold et al., Secomb et al., and Lorthois et al. all constructed accurate cerebral capillary networks directly from experimental data (Lorthois et al., 2011; Reichold et al., 2009; Secomb et al., 2000). Such networks are difficult to scale-up discretely due to the rapidly increasing computational cost as voxel size increases. The choice of boundary condition also has a very significant effect on the flow solution. Reichold et al. homogenized a 2-dimensional idealised model of the cerebral capillary bed, where all capillaries have the same diameter. The model built upon here, in contrast, conforms statistically to morphometric data, is 3-dimensional, and the homogenized flow solutions are independent of the choice of boundary condition. Additionally, the model here has been used to characterise the effect of the microvasculature on tissue-scale blood flow to allow for the construction of larger scale cerebral blood flow models. Such information has been previously unavailable.

In a similar study, Smith et al. used the same homogenization methods applied here on synthetic rat coronary capillary networks (Smith et al., 2014). The network was assumed to be 2-dimensional with orthogonal connections between capillaries. They found that as the voxel size of the capillary network increases, the permeability drops and eventually converges. This is also found here for the principal terms, although the magnitude of the drop is found to be smaller than that for a coronary network. This was due to the much more complex, less-dense, random nature of the cerebral microvasculature reducing the variability of flow with varying cube size. Smith et al. also found that the permeability of the network is of order 10^{-3} mm^3 s kg^{-1} in the longitudinal direction and of order 10^{-4} mm^3 s kg^{-1} in the cross capillary direction. We found that the permeability for the cerebral microvasculature is of order 10^{-4} mm^3 s kg^{-1} in all three orthogonal directions, in agreement with the cross-capillary direction (which had a similar order magnitude density as our capillary network). As the larger permeability found in Smith et al. is attributed as compensating for the compression of the capillaries, and hence restricted flow in systole, then it would appear that a permeability of order 10^{-4} mm^3 s kg^{-1} is enough both in the heart and brain to maintain healthy function.

One limitation of the model is the assumption of periodicity of the microvascular network. This assumption was made to simplify the derivation of the homogenized equations; however it is not yet known whether such an assumption is valid for the cerebral microvasculature. It can be argued that for a sufficiently random microstructure, the approximation of periodicity is a good assumption (Auriault, 2011; Holmes, 2013). In the absence of experimental data determining the randomness or periodicity of the capillary networks, periodicity is used to simplify the derivation.

It should be noted that the network generation algorithm used here is based on one set of experimental morphometric data (Cassot et al., 2006) (due to the lack of other accurate data on the cerebral microvasculature). Therefore, the permeability tensor calculated in this paper characterises only a small region of the brain. The network topology and density may vary substantially within the brain, being closely linked with functional activity. However, as the algorithm is statistically based, it would easily be possible to modify it for different sets of morphometric data, and to use the same homogenization procedure laid out in this paper to characterise the permeability of different regions. As more information about the topology and geometry of cerebral microvascular networks becomes available, the more it will be possible to effectively and accurately characterise other regions of the brain.

The blood flow model here assumed a constant hematocrit throughout the capillary network; hence the viscosity in each capillary was only dependent on vessel diameter. It is known, however, that at bifurcations and trifurcations in the network, plasma skimming (or phase separation) takes place, where red blood cells are distributed unevenly across the daughter vessels. This leads to changes in hematocrit throughout the capillary network. This effect has been quantified (Pries et al., 1989), but was omitted in this paper. Su applied this variable hematocrit model to his microvascular model (Su, 2011). He found the vessel flow rates were on average 20 % smaller in comparison to the constant hematocrit model. However, there was no significant qualitative difference in flow distribution patterns. A variable hematocrit model will be incorporated in future work.

The current discrete model adapted here (Su et al., 2012) is able to model voxel sizes of up to 625 µm before becoming computationally too expensive on a standard PC. In order

to make comparisons with clinical data, voxel sizes of the order mm will need to be generated. Imaging voxels are usually of the order mm^3 in volume. Such a volume will contain, as well as capillaries, larger structures such as arterioles and venules. If any accurate comparison is to be made between clinical or experimental perfusion data and the model, arterioles and venules must be incorporated into the model in the future, whilst maintaining periodicity.

The method presented here provides a novel technique to 'scale-up' such discrete networks and to calculate the permeability tensor $\mathbf{K}$. This tensor provides fundamental information about the network flow conductivity and can be used to parameterise large models of the microvasculature. Modelling larger volumes of the brain is important for understanding whole-organ cerebral flow. The permeability tensor calculated here represents capillary bed flow conductivity under normal conditions. The framework developed however, could also be used to quantify the effects of microvascular changes in the brain. Of particular interest is ischemic stroke, where a statistically accurate network model is already in place (Park and Payne, 2013). The current stroke model is discrete and only able to model cube sizes of 250 μm. Applying the techniques laid out in this paper will allow us better to determine the effects of ischemic stroke on the permeability of the capillary beds, as well as to build larger scale models to compare with imaging voxel data.

5. Conclusions

This study has characterised the tissue-scale permeability of the cerebral microvasculature. Mathematical averaging techniques were combined with a statistical,

periodic, anatomical model of the cerebral capillary bed to determine the permeability tensor. Calculation of the permeability tensor enables characterisation of the microvasculature flow properties to be performed at a specific region in the brain. This can then be used to build larger models of perfusion which can in turn be compared to voxel data for validation. The techniques laid out in this paper could be used to scale-up other microvascular topologies and densities. This will allow larger regions of the brain to be modelled, helping us further to understand the link between the microstructure and global perfusion. The permeability tensor has been shown to converge to some effective permeability (K_{eff}) at larger voxel sizes, as well as to be isotropic, reflecting the mesh-like structure of the capillary network on the micro-scale. The off-diagonals are normally distributed about zero. These results parameterise the microvasculature for a region of the brain, and allow larger scale continuum models to be built. Future work will involve adding arterioles and venules to the statistical discrete model of the microvasculature, in order to provide an accurate comparison of modelled perfusion values and perfusion values extracted from imaging data.

6. Acknowledgments

W. K. El-Bouri is funded by an EPSRC DTP studentship

7. References

Auriault, J.-L., Boutin, C., Geindreau, C., 2009. Homogenization of Coupled Phenomena in Heterogeneous Media. Wiley ISTE, London.

Auriault, J. L., 2011. Heterogeneous periodic and random media. Are the equivalent macroscopic descriptions similar? International Journal of Engineering Science 49, 806-808, doi:http://dx.doi.org/10.1016/j.ijengsci.2011.01.005.

Bear, J., 1988. Dynamics of Fluids in Porous Media. Dover Publications.

Cassot, F., Lauwers, F., Fouard, C., Prohaska, S., Lauwers-Cances, V., 2006. A novel three-dimensional computer-assisted method for a quantitative study of microvascular networks of the human cerebral cortex. Microcirculation 13, 1-18, doi:10.1080/10739680500383407.

Clarke, D. D., Sokoloff, L., 1999. Circulation and Energy Metabolism of the Brain. Basic Neurochemistry: Molecular, Cellular and Medical Aspects. Lippincott-Raven, Philadelphia, pp. 645-680.

Dekaban, A. S., Sadowsky, D., 1978. Changes in brain weights during the span of human life: Relation of brain weights to body heights and body weights. Annals of Neurology 4, 345-356, doi:10.1002/ana.410040410.

Durlofsky, L. J., 1991. Numerical calculation of equivalent grid block permeability tensors for heterogeneous porous media. Water Resources Research 27, 699-708, doi:10.1029/91WR00107.

Fang, Q., Sakadzic, S., Ruvinskaya, L., Devor, A., Dale, A. M., Boas, D. A., 2008. Oxygen advection and diffusion in a three-dimensional vascular anatomical network. Optics Express 16, 17530-17541, doi:10.1364/OE.16.017530.

Holmes, M. H., 2013. Introduction to Perturbation Methods. Springer New York, New York.

Lauwers, F., Cassot, F., Lauwers-Cances, V., Puwanarajah, P., Duvernoy, H., 2008. Morphometry of the human cerebral cortex microcirculation: general characteristics and space-related profiles. Neuroimage 39, 936-48, doi:10.1016/j.neuroimage.2007.09.024.

Lorthois, S., Cassot, F., Lauwers, F., 2011. Simulation study of brain blood flow regulation by intra-cortical arterioles in an anatomically accurate large human vascular network: Part I: methodology and baseline flow. Neuroimage 54, 1031-42, doi:10.1016/j.neuroimage.2010.09.032.

Lüders, E., Steinmetz, H., Jäncke, L., 2002. Brain size and grey matter volume in the healthy human brain. NeuroReport 13, 2371-2374.

Obrist, W. D., Thompson, H. K., King, H., Wang, H. S., 1967. Determination of Regional Cerebral Blood Flow by Inhalation of 133-Xenon. Circulation Research 20, 124-135, doi:10.1161/01.res.20.1.124.

Park, C. S., Payne, S. J., 2013. A generalized mathematical framework for estimating the residue function for arbitrary vascular networks. Interface Focus 3, 20120078, doi:10.1098/rsfs.2012.0078.

Pries, A. R., Ley, K., Claassen, M., Gaehtgens, P., 1989. Red cell distribution at microvascular bifurcations. Microvasc Res 38, 81-101.

Pries, A. R., Secomb, T. W., Gessner, T., Sperandio, M. B., Gross, J. F., Gaehtgens, P., 1994. Resistance to blood flow in microvessels in vivo. Circ Res 75, 904-15.

Reichold, J., Stampanoni, M., Lena Keller, A., Buck, A., Jenny, P., Weber, B., 2009. Vascular graph model to simulate the cerebral blood flow in realistic vascular networks. J

Cereb Blood Flow Metab 29, 1429-1443, doi:http://www.nature.com/jcbfm/journal/v29/n8/suppinfo/jcbfm200958s1.html.

Renard, P., de Marsily, G., 1997. Calculating equivalent permeability: a review. Advances in Water Resources 20, 253-278, doi:10.1016/S0309-1708(96)00050-4.

Sakadžić, S., Mandeville, E. T., Gagnon, L., Musacchia, J. J., Yaseen, M. A., Yucel, M. A., Lefebvre, J., Lesage, F., Dale, A. M., Eikermann-Haerter, K., Ayata, C., Srinivasan, V. J., Lo, E. H., Devor, A., Boas, D. A., 2014. Large arteriolar component of oxygen delivery implies a safe margin of oxygen supply to cerebral tissue. Nat Commun 5, doi:10.1038/ncomms6734.

Secomb, T. W., Hsu, R., Beamer, N. B., Coull, B. M., 2000. Theoretical simulation of oxygen transport to brain by networks of microvessels: effects of oxygen supply and demand on tissue hypoxia. Microcirculation 7, 237-47.

Shipley, R. J., Chapman, S. J., 2010. Multiscale Modelling of Fluid and Drug Transport in Vascular Tumours. Bulletin of Mathematical Biology 72, 1464-1491, doi:10.1007/s11538-010-9504-9.

Smith, A. F., Shipley, R. J., Lee, J., Sands, G. B., LeGrice, I. J., Smith, N. P., 2014. Transmural variation and anisotropy of microvascular flow conductivity in the rat myocardium. Ann Biomed Eng 42, 1966-77, doi:10.1007/s10439-014-1028-2.

Su, S. W., 2011. Modelling Blood Flow and Oxygen Transport in the Human Cerebral Cortex. DPhil Thesis, University of Oxford.

Su, S. W., Catherall, M., Payne, S., 2012. The influence of network structure on the transport of blood in the human cerebral microvasculature. Microcirculation 19, 175-87, doi:10.1111/j.1549-8719.2011.00148.x.

Appendix A. Homogenization of Stokes Flow

We briefly present here the homogenization of Stokes flow. Since we are assuming scale separation between the micro and macro length scales ($\varepsilon \ll 1$), the macro length scale can be defined in terms of the micro length scale as $\mathbf{x} = \varepsilon\mathbf{X}$. Therefore both $\mathbf{x}$ and $\mathbf{X}$ can be treated as independent variables and so:

$$\nabla = \nabla_{\mathbf{X}} + \varepsilon\nabla_{\boldsymbol{x}}\,, \quad \nabla^2 = \nabla_{\mathbf{X}}^{\mathbf{2}} + 2\varepsilon\nabla_{\boldsymbol{x}}.\nabla_{\mathbf{X}} + \varepsilon^2\nabla_{\boldsymbol{x}}^2 \tag{A.1}$$

Using (A.1) in (6) and (2) leads to:

$$-\nabla_{\mathbf{X}}p_c - \varepsilon\nabla_{\boldsymbol{x}}p_c + \varepsilon\nabla_{\mathbf{X}}^{\mathbf{2}}\mathbf{u}_c + 2\varepsilon^2\nabla_{\boldsymbol{x}}.\nabla_{\mathbf{X}}\mathbf{u}_c + \varepsilon^3\nabla_{\boldsymbol{x}}^{\mathbf{2}}\mathbf{u}_c = 0 \tag{A.2}$$

$$\nabla_{\mathbf{X}}.\,\mathbf{u}_c + \varepsilon\nabla_{\boldsymbol{x}}.\,\mathbf{u}_c = 0 \tag{A.3}$$

with the no-slip, no-leak boundary conditions unchanged. A multiple scales expansion of the form:

$$\begin{aligned}\mathbf{u}_c &= \mathbf{u}_c^{(0)}(\mathbf{x},\mathbf{X}) + \varepsilon\mathbf{u}_c^{(1)}(\mathbf{x},\mathbf{X}) + \varepsilon^2\mathbf{u}_c^{(2)}(\mathbf{x},\mathbf{X}) + \cdots \\ p_c &= p_c^{(0)}(\mathbf{x},\mathbf{X}) + \varepsilon p_c^{(1)}(\mathbf{x},\mathbf{X}) + \varepsilon^2 p_c^{(2)}(\mathbf{x},\mathbf{X}) + \cdots\end{aligned} \tag{A.4}$$

is substituted into the above equations, with successive orders of ε equated in order to determine the leading order homogenized equations for capillary flow and pressure. In order to maintain periodicity each component of $\mathbf{u}_c$ and p_c is periodic in $\mathbf{X}$.

Equating powers of $\mathcal{O}(1)$ in equations (A.2) and (A.3) gives:

$$\nabla_{\mathbf{X}} p_c^{(0)} = 0, \quad \nabla_{\mathbf{X}} . \mathbf{u}_c^{(0)} = 0 \tag{A.5}$$

and equating powers of $\mathcal{O}(\varepsilon)$ gives:

$$\nabla_{\mathbf{X}} p_c^{(1)} + \nabla_{\boldsymbol{x}} p_c^{(0)} = \nabla_{\mathbf{X}}^{\mathbf{2}} \mathbf{u}_c \,, \quad \nabla_{\mathbf{X}} . \mathbf{u}_c^{(1)} + \nabla_{\boldsymbol{x}} . \mathbf{u}_c^{(0)} = 0 \tag{A.6}$$

From (A.5) it is evident that $p_c^{(0)}$ is constant at the local scale. In order to determine the leading order problem it is necessary to solve for $\mathbf{u}_c^{(0)}$ and $p_c^{(1)}$. From (A.6) it can be seen that $\mathbf{u}_c^{(0)}$ and $p_c^{(0)}$ are both linear functions of $\nabla_{\boldsymbol{x}} p_c^{(0)}$ and so solutions are proposed of the form:

$$\mathbf{u}_c^{(0)} = -\boldsymbol{w}_c^j(\mathbf{X}) \frac{dp_c^{(0)}}{dx^j} \tag{A.7}$$

$$p_c^{(1)} = -P_c^j(\mathbf{X}) \frac{dp_c^{(0)}}{dx^j} + \bar{p_c}^{(1)} \tag{A.8}$$

where j can take the values 1, 2, or 3 and refers to the Cartesian co-ordinate directions, and $\boldsymbol{w}_c^j(\mathbf{X})$ and $P_c^j(\mathbf{X})$ account for the local variations in $\mathbf{u}_c^{(0)}$ and $p_c^{(1)}$ and are known as the cell variables. Inserting the proposed solutions into (A.5) and (A.6) leaves us with the cell problem:

$$\nabla_{\mathbf{X}} . \boldsymbol{w}_c^j(\mathbf{X}) = 0 \,, \quad \nabla_{\mathbf{X}} P_c^j(\mathbf{X}) = \nabla_{\mathbf{X}}^{\mathbf{2}} \boldsymbol{w}_c^j(\mathbf{X}) + \mathbf{e}_{\mathrm{j}} \quad \text{in } \Omega_c \tag{A.9}$$

with no-slip, no-leak boundary conditions in terms of $\boldsymbol{w}_c^j(\mathbf{X})$, and $\mathbf{e}_{\mathrm{j}}$ being the unit vector in the j-direction. This is the local periodic cell problem which must be solved numerically in order to derive the parameters of the macro scale problem. The local pressure term is only defined up to a constant value and so a uniqueness condition is imposed which states that the volume average of P_c^j is zero.

Taking a volume average over $\mathbf{u}_c^{(0)}$ (A.7) results in:

$$\langle \mathbf{u}_c^{(0)} \rangle_{\Omega_c} = -\mathbf{K} \nabla_{\boldsymbol{x}} p_c^{(0)} \tag{A.10}$$

where

$$K_{ij} = \frac{1}{|\Omega|} \int_{\Omega_c} w_{ci}^j \, dV \tag{A.11}$$

This is Darcy's Law with $\mathbf{K}$ defining the permeability tensor. Therefore, to leading order, the homogenization of the Stokes equation results in Darcy's Law.

Finally, consider the expanded incompressibility equation in (A.6) and volume average over the fluid domain. Using the divergence theorem, along with the no-slip condition and periodicity of $\mathbf{u}_c^{(1)}$ leads to the macro-scale volume conservation equation

$$\nabla_{\boldsymbol{x}} \cdot \langle \mathbf{u}_c^{(0)} \rangle = 0 \tag{A.12}$$

Highlights

- Homogenization of statistically accurate human cerebral capillary networks.
- A converged, isotropic permeability is determined as cube size increases.
- A REV of 375 μm found to give error of 4.5% from converged permeability.
- The permeability gives a CBF in agreement with experimental values.
- Opens up possibility of large scale cerebral blood flow models.